CrystEngComm

Accepted Manuscript

ROYAL SOCIETY OF CHEMISTRY

www.rsc.org/crystengcomm

Polymorphism in anti-hyperammonemic agent N-carbamoyl-L-glutamic acid†

D. Maddileti, and Ashwini Nangia*
School of Chemistry, University of Hyderabad, Prof. C. R. Rao Road, Gachibowli, Central University PO, Hyderabad 500 046, India.
E-mail: ashwini.nangia@gmail.com

Abstract
Carglumic acid (CGA) is used for the treatment of hyperammonaemia. The aim of this study was to investigate novel crystalline forms of CGA which can offer improved physicochemical properties and also to understand the stability relationships between such forms. We report two novel polymorphs I and II, and a degradation derivative of the drug hydantoin-5-propionic acid (5-HPA). Crystallization conditions have been optimized to obtain each polymorph in reproducible crystallization batches. 5-HPA was obtained serendipitously upon crystallization of CGA in acidic medium (2-butanone : propionic acid). The X-ray crystal structure of CGA Form-I and II and 5-HPA are sustained by carboxylic acid catemer and dimer, carboxamide catemer and dimer and acid–amide heterosynthon. The two polymorphs are monotropically related. Thermodynamic stability, phase transformation, and Hirshfeld surface maps complement the structural analysis. Both forms are stable for two months in accelerated ICH conditions of 40 ºC and 75% RH. Dynamic vapor sorption (DVS) showed that Form-I is more stable to moisture conditions than Form-II. Slurry crystallization, mechanical grinding and thermal measurements confirm the thermodynamic nature of CGA Form-I.

† Electronic Supplementary Information with this paper. Molecular torsion angles, IR and NMR spectra shifts, and PXRD overlay plots.

Introduction

Carglumic acid is an orphan drug used for the treatment of hyperammonaemia in patients with N-acetylglutamate synthase (NAGS) deficiency.[1] NAGS deficiency is one the most severe and rarest of the hereditary urea cycle disorders (UCDs). This rare genetic disorder results in elevated levels of ammonia in the blood, which can eventually cross the blood-brain barrier and cause neurologic problems, cerebral edema, coma, and eventually death. CGA is a structural analogue of N-acetylglutamate, the naturally occurring activator of carbamoyl phosphate synthetase (CPS) and helps to break down ammonia to reduce concentration in blood and toxic effects.[2] CGA was approved by the U.S. Food and Drug Administration (FDA) in 2010 to treat hyperammonemia because it can act as a replacement for NAG in NAGS deficient patients by activating CPS.[3] It is sold under brand name Carbaglu® which is formulated as a water-dispersible tablet and each tablet contains 200 mg of carglumic acid and excipients. CGA is an acidic drug molecule in the form of white crystalline powder having aqueous solubility of 19.1 mg/mL[4] and practically insoluble in organic solvents, perhaps due to high density of functional groups (dicarboxylic acid and urea) in a small molecule. Studies on hyperammonemia are limited due to the rarity of the disease. The condition is particularly toxic to the central nervous system (CNS).[5] X-ray crystal structure of the analog N-acetylglutamate is reported[6] (CSD Refcode TERRUD and TERRUD01, multiple determinations of the same structure), but no crystal structure of CGA was found in the Cambridge Structural Database (ver. 5.36, November 2014 update).[7] In view of the importance of polymorphism in pharmaceuticals[8] to control physicochemical properties, solubility, stability, dissolution rate, melting point, bioavailability,[9] etc., CGA was screened by different techniques such as liquid-assisted grinding (LAG), slurry crystallization, solvent removal in rotavap, freeze drying, spray drying, and solution crystallization.[10] Two novel polymorphs named Form-I, and Form-II and a degraded derivative of CGA, hydantoin-5-propionic acid are reported (5-HPA, chemical name 3-(2,5-dioxoimidazolidin-4-yl) propanoic acid).

Results and Discussion

Since the API is routinely exposed to various conditions ranging from production to tableting to transportation before consumption, the risk of process-induced transformations and stability of polymorphs must be properly understood for phramaceuticals.[11] Thus, a sound understanding of a polymorphic system is a prerequisite for product quality and performance. Even though strong hydrogen bonding functional groups COOH and urea are present in CGA molecule, which generally promote crystallization, we had to try a range of solvent systems and mixtures to obtain diffraction quality crystals. A majority of crystallization experiments gave microcrystalline powders which matched with the PXRD pattern of the starting material (Form-I). Solubility of CGA in aqueous medium is very high but in organic solvents it is practically insoluble. This limitation narrowed down the variety of solvents which could be used for crystallization screen, and hence mostly Form-I was observed. Form-I was crystallized by slurring the starting compound in EtOH, freeze drying in water (lyophilization), and spray drying from water. Novel Form-II was produced upon rotovaporization of CGA in water: acetone (1:5 v/v solvent) (see

Experimental Section). The above procedures were optimized to obtain reproducibly pure polymorphs I and II. A degradation derivative of CGA, 5-HPA, was serendipitously obtained upon solution crystallization of CGA from 2-butanone: propionic acid (1:1 v/v) (Scheme 1). The three crystal structures illustrate acid-acid catemer and dimer, amide-amide homodimer, and acid-amide heterosynthons[12] (Scheme 2). In this paper we describe X-ray crystal structures of two novel forms and one degraded form of CGA, which are fully characterized by spectroscopic (FT-IR, ^{13}C ss-NMR), thermal (DSC), field emission scanning electron microscopy (FESEM), powder X-ray diffraction (PXRD), and their structures were confirmed by single crystal X-ray diffraction. Crystallographic parameters of the novel forms and their hydrogen bonds are listed in Table 1 and Table 2.

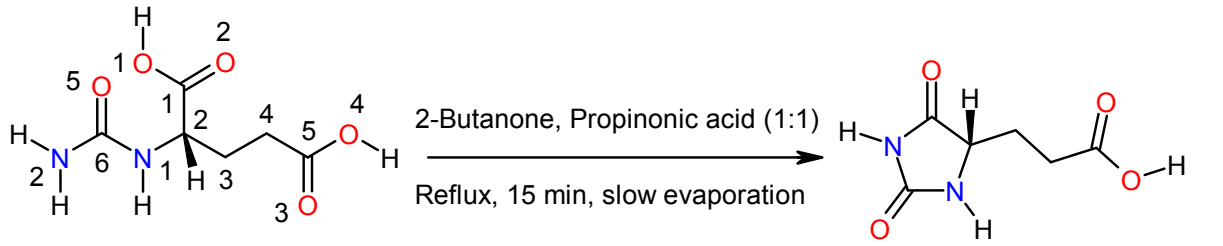

L-Carglumic acid, CGA Hydantoin-5-propionic acid, 5-HPA

Scheme 1 The transformation of CGA to 5-HPA during crystallization. The natural L-glutamic acid S-configuration is shown.

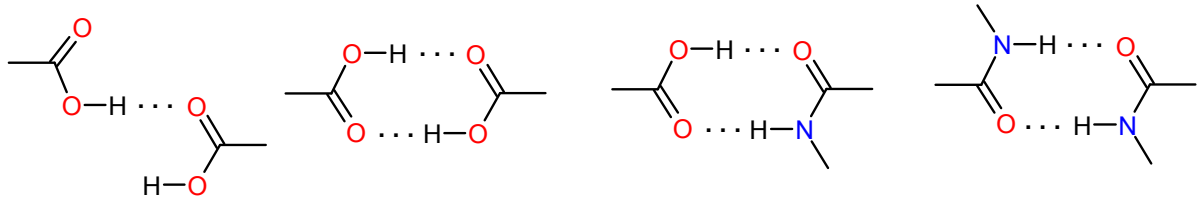

Scheme 2 Hydrogen bonded synthons in crystal structures.

The chemical structure of CGA (Scheme 1) indicates that the conformationally flexible molecule will exhibit different torsion angles. The two symmetry-independent molecules in the asymmetric unit of Form-II are labeled A and B. The values of τ_1 (C2-C3-C4-C5) and τ_2 (C6-N1-C2-C1) are 79.7°(2), 81.26°(16) in Form-I, and 177.4°(1), −55.8°(2) for molecule A, and 178.7°(1), −57.6°(2) of molecule B in Form-II respectively. The main difference in the torsion angles of both Forms-I and II was observed for τ_1 in the alkyl chain portion (C2-C3-C4-C5 $\Delta\tau$ about 100°, see Table S1, ESI†) for these conformational polymorphs.[13] The overlay diagram of the CGA molecules from Form-I and II shows conformational changes (Figure 1). From the molecular overlay and structural analysis we can classify both forms as conformational and synthon polymorphs. Reflections data were collected using Mo-Kα X-radiation and the S-

configuration at the chiral center in the molecule was assigned based on the natural L-glutamic acid derived starting material.

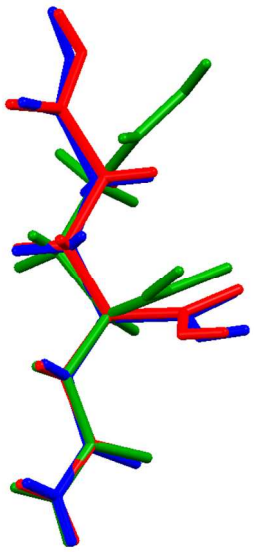

Figure 1 Overlay diagram of CGA molecules in Form-I and II. Color code: Green = Form-I, Red = CGA-Form-IIA, Blue = CGA-Form-IIB. Note that A and B are the two symmetry-independent molecules in the crystal structure of the Form-II.

Crystal structure analysis

Form-I

Upon crystallizing commercial pharmaceutical grade CGA from MeOH : 2-butanone (1:1 v/v) needle shaped crystals were obtained which solved and refined in the orthorhombic space group $P2_12_12_1$. CGA molecules are connected by the acid catemer synthon of C(4) graph set notation,[14] which is stabilized by C–H···O (2.58 Å, 144º) interaction resulting in a 1D tape along [100] (Figure 2a). The second carboxylic acid and N-carbamoyl groups are connected through N–H···O=C (acid) (1.90 Å, 167º) and N–H···O=C (carbamoyl) (2.09 Å, 147º) H-bonds resulting in R_2^2 (11) motif.[14] Such tapes are inter-connected through acid-amide R_2^2 (8) heterosynthon in a corrugated sheet structure (Figure 2b).

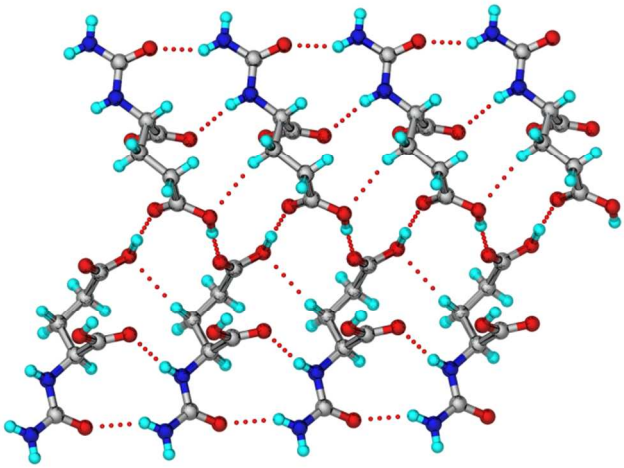

(a)

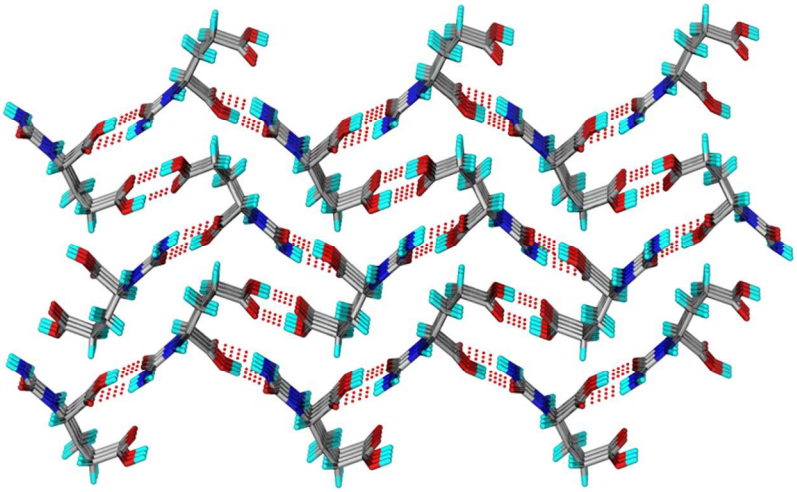

(b)

Figure 2 (a) 1D tape formed through acid-acid C(4) catemer and supporting C–H···O and N–H···O interactions. (b) Acid-acid C(4) chain and acid-amide $R_2^2(8)$ heterosynthon result in a corrugated structure.

Form-II

Crystallization of CGA from CH_3CN : m-cresol (1:1 v/v) mixture afforded block crystals which were solved and refined in the monoclinic space group *P2₁* with two molecules of CGA in the asymmetric unit. One of the carboxylic acid and N-carbamoyl group of CGA forms acid-amide $R_2^2(8)$ motif (N–H···O: 1.90 Å, 167º; 1.94 Å, 160º; O–H···O: 1.63 Å, 172º; 1.66 Å, 170º) resulting in an infinite linear chain along the [001] direction (Figure 3a). These chains extend in a 2D sheet parallel to the (020) plane, being connected to the other carboxylic acid and carbamoyl group through N–H···O=C (acid) (1.82 Å, 173º; 1.86 Å, 156º) and N–H···O=C (carbamoyl) (2.21 Å, 147º; 2.25 Å, 146º) bonds (Figure 3b). Adjacent sheets are connected

through O–H···O (1.73 Å, 166º; 1.73 Å, 166º) hydrogen bonds resulting in ladder like structure, and C−H···C short contacts connect these ladders (Figure 3c).

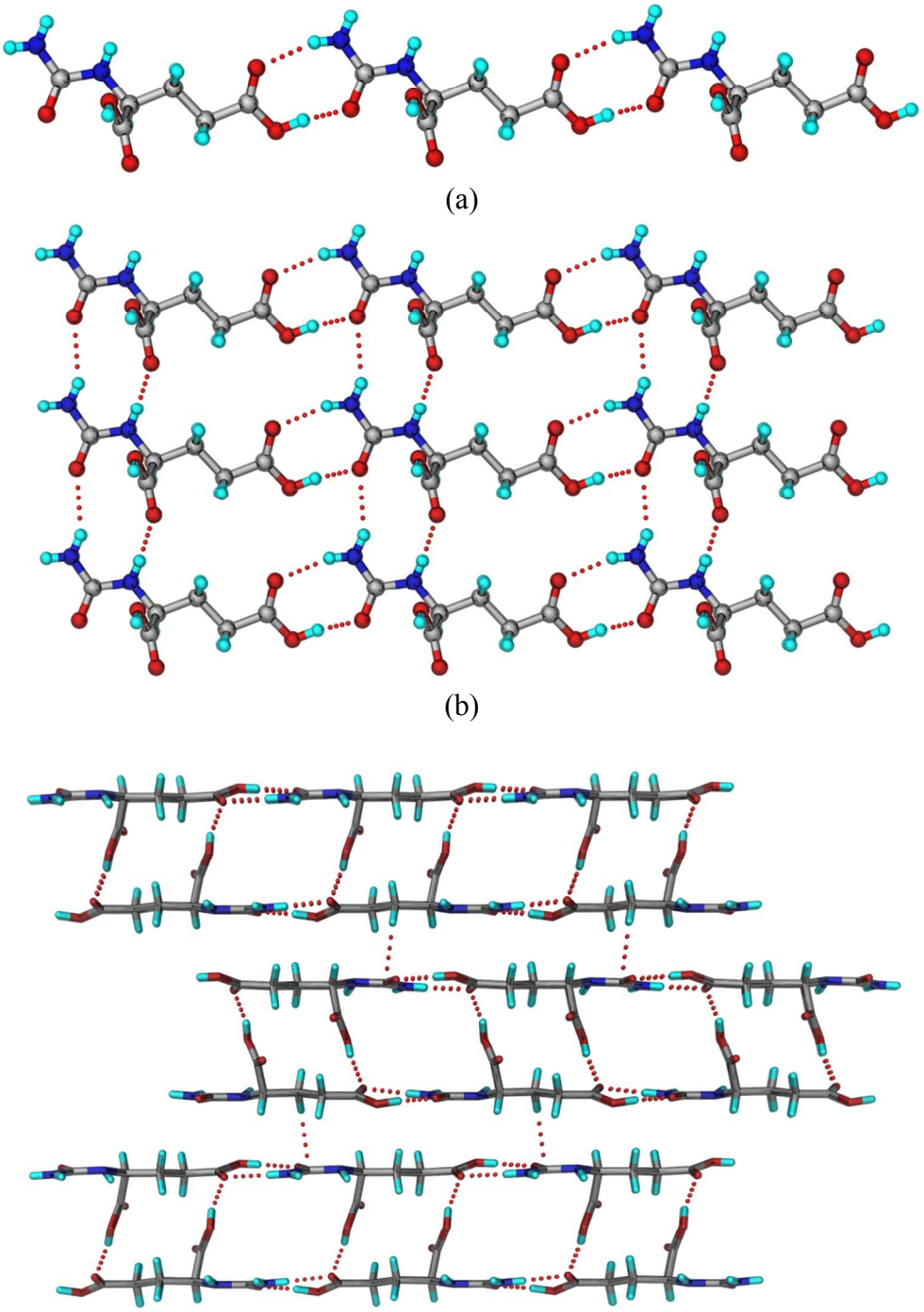

Figure 3 (a) An infinite linear chain formed through acid-amide $R_2^2(8)$ heterosynthon. (b) Hydrogen bonded 2D sheet structure formed through N–H···O interactions. (c) O–H···O and C−H···π interactions in the inter-sheet region viewed down the a-axis.

Hydantoin-5-propionic acid (5-HPA)

Hydantoin-5-propionic acid (5-HPA, chemical name 3-(2,5-dioxoimidazolidin-4-yl) propanoic acid) was obtained as a by-product of crystallization of CGA from 2-butanone : propionic acid (1:1 v/v) solvent mixture. The structure was solved and refined in monoclinic space group $P2_1$ with two molecules of 5-HPA in the asymmetric unit. The molecules form an infinite linear chain through acid-acid $R_2^2(8)$ (O–H···O: 1.72 Å, 171º; 1.74 Å, 172º) and amide-amide $R_2^2(8)$ (N–H···O: 1.79 Å, 171º; 1.81 Å, 161º) homosynthons. Such chains are inter-connected through N–H···O (1.88 Å, 168º; 1.89 Å, 176º) and C–H···O (2.58 Å, 161º; 2.62 Å, 144º) H-bonds in a corrugated 2D sheet, with weak C–H···O (2.48 Å, 139º; 2.53 Å, 137º; 2.29 Å, 145º) interactions to complete the structure (Figure 4).

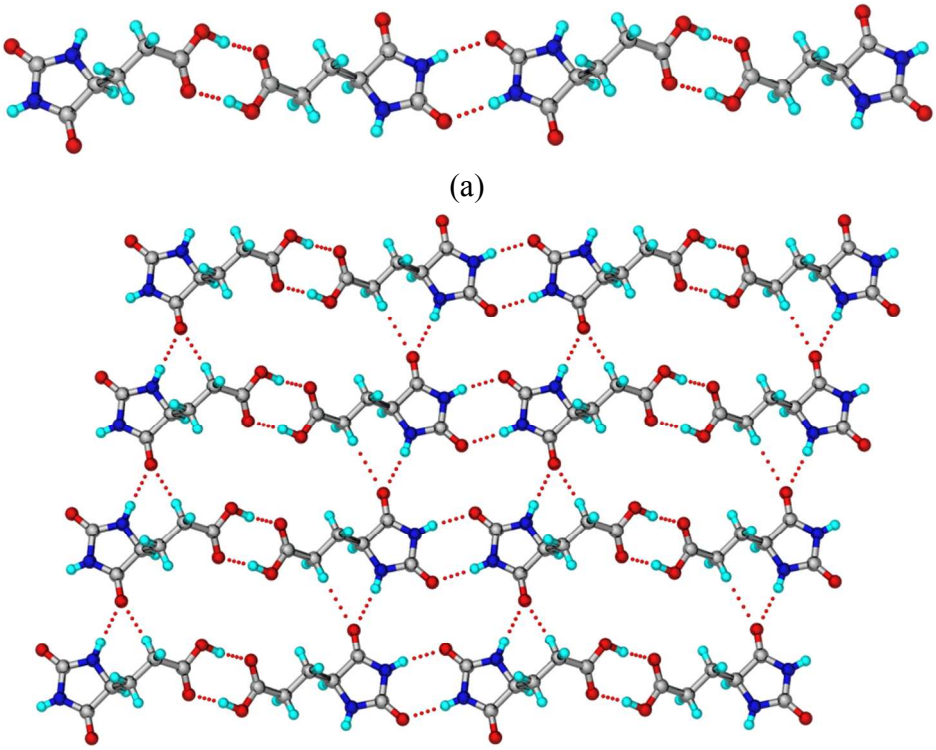

(a)

(b)

Figure 4 (a) Infinite linear chain formed through acid-acid $R_2^2(8)$ and amide-amide $R_2^2(8)$ homosynthons. (b) A 2D corrugated sheet structure assembled through N–H···O and C–H···O interactions.

Table 1 Cystallographic parameters of CGA polymorphs and 5-HPA.

	CGA–Form-I	CGA–Form-II	Hydantoin-5-propionic acid (5-HPA)
chemical formula	C6 H10 N2 O5	C6 H10 N2 O5	C6 H8 N2 O4
formula weight	190.16	190.16	172.14
crystal system	Orthorhombic	monoclinic	monoclinic
space group	$P2_12_12_1$	$P2_1$	$P2_1$
T [K]	100(2)	100(2)	298(2)
a [Å]	5.1179(8)	5.3615(5)	6.2475(4)
b [Å]	12.2079(18)	15.8123(15)	7.1111(6)
c [Å]	12.7508(19)	9.9631(9)	17.3692(11)
α [°]	90	90	90
β [°]	90	90.899(2)	96.792(5)
γ [°]	90	90	90
Z	4	4	4
V [Å^3]	796.7(2)	844.54(14)	766.24(10)
D_{calc} [g cm^{-3}]	1.585	1.496	1.492
M [mm^{-1}]	0.139	0.131	0.127
Reflns. collected	8323	8820	3079
Unique reflns.	1576	3335	2191
Observed reflns.	1532	3159	1973
R_1 [I>2(I)]	0.0264	0.0323	0.0362
wR_2 (all)	0.0632	0.0777	0.0804
Goodness-of-fit	1.089	1.049	1.068
Diffractometer	Bruker SMART Apex	Bruker SMART Apex	Oxford CCD

Table 2 Hydrogen bond metrics in crystal structures.

Interaction	H···A (Å)	D···A (Å)	D–H···A (º)	Symmetry Code
CGA–Form-I				
O1–H1···O5	1.63	2.548(1)	167	-x+1,+y+1/2,-z+1/2+1
O4–H5···O3	1.72	2.660(2)	176	x-1/2,-y+1/2+2,-z+1
N1–H6···O2	1.90	2.914(2)	167	x+1,+y,+z
N2–H2A···O5	2.09	3.009(2)	147	x+1,+y,+z
N2–H2B···O2	2.09	3.084(2)	161	-x+1,+y-1/2,-z+1/2+1
C3–H3A···O4	2.58	3.515(2)	144	x+1,+y,+z
CGA–Form-II				
O1–H1···O8	1.73	2.662(2)	171	x,y,z
O4–H5···O5	1.66	2.587(2)	170	x,+y,+z-1
O6–H7···O3	1.73	2.664(2)	166	x-1,+y,+z

O9–H11···O10	1.63	2.558(2)	172	x,+y,+z+1
N1–H6···O2	1.82	2.841(2)	173	x+1,+y,+z
N2–H2A···O5	2.25	3.159(2)	146	x+1,+y,+z
N2–H2B···O3	1.90	2.915(2)	167	x,+y,+z+1
N3–H12···O7	1.86	2.832(2)	156	x+1,+y,+z
N4–H13A···O8	1.94	2.931(2)	160	x,+y,+z-1
N4–H13B···O10	2.21	3.119(2)	147	x+1,+y,+z
C4–H4A···O6	2.39	3.299(2)	141	x,y,z
C9–H9B···O2	2.63	3.505(2)	138	x,y,z
C10–H10A···O1	2.44	3.381(2)	145	x-1,+y,+z
Hydantoin-5-propionic acid (5-HPA)				
O1–H1···O6	1.72	2.646(3)	171	x, y, z
O5–H7···O2	1.74	2.670(3)	172	x, y, z
N1–H5···O4	1.89	2.914(2)	176	x-1,+y,+z
N2–H6···O7	1.79	2.820(2)	171	x+1,+y, +z+1
N3–H11···O8	1.88	2.900(2)	168	x+1,+y,+z
N4–H12···O3	1.81	2.801(2)	161	x-1,+y,+z-1
C2–H2A···O1	2.29	3.239(4)	145	-x+1,+y-1/2,-z+1
C2–H2B···O4	2.58	3.618(3)	161	x-1,+y,+z
C3–H3A···O5	2.53	3.397(3)	137	-x+2,+y-1/2,-z+1
C8–H8A···O8	2.62	3.551(3)	144	x+1,+y,+z
C10–H10···O3	2.48	3.365(3)	139	-x+1,+y+1/2,-z+1

Spectroscopic characterization

IR spectroscopic analysis of CGA forms showed significant differences in the vibrational patterns of their functional groups.[15] The NH_2 asymmetric stretch of $C(=O)NH_2$ in Form-I gives a strong band at 3439.9 cm^{-1} and symmetric NH_2 stretch at 3344.3 cm^{-1} with a somewhat weaker intensity, whereas for secondary NH stretch it showed peaks at 3295.4 cm^{-1}. The asymmetric and symmetric stretching frequencies of $C(=O)NH_2$ in Form-II appeared at 3454.3 cm^{-1} and 3315.3 cm^{-1}, and for secondary NH at 3247.3 cm^{-1}. The C=O stretching vibration the carboxylic acid gave a strong absorption at 1728.5 cm^{-1} in Form-I and 1709.9 cm^{-1} in Form-II. The stretching frequencies for amide C=O resonated at 1697.3 cm^{-1} in Form-I and 1666.9 cm^{-1} in Form-II. The signature frequencies are listed in Table S2 (see ESI†) and spectra are presented in Figure 5.

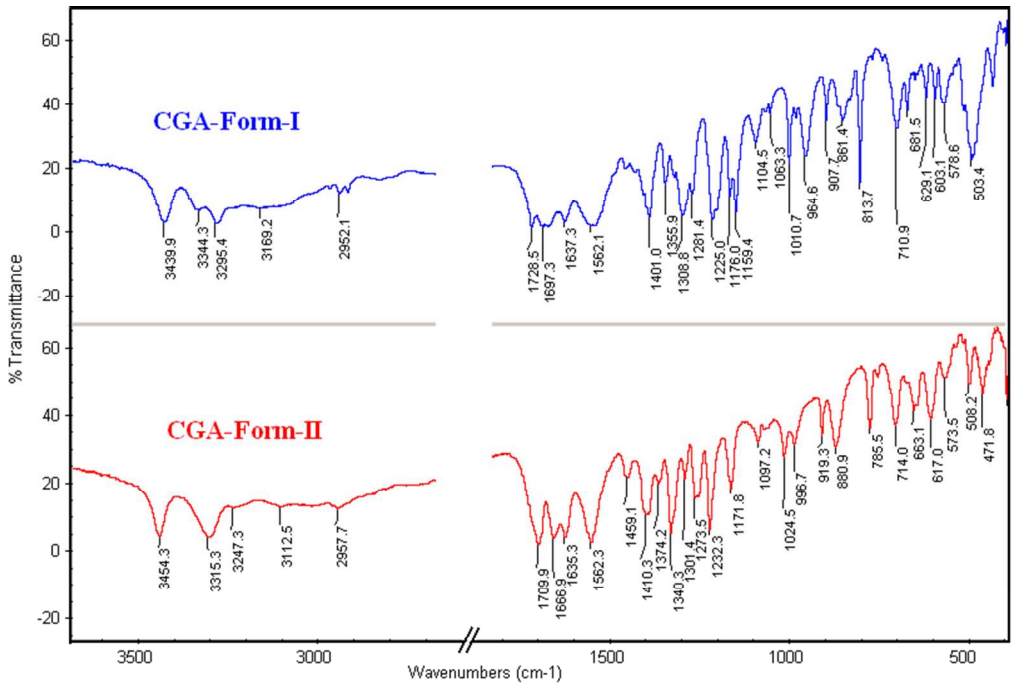

Figure 5 FT-IR spectral comparison of CGA forms indicate that there is significant differences in stretching frequencies between the two polymorphs.

We also characterized CGA forms through solid-state NMR because this technique provides information about differences in hydrogen bonding, molecular environment, and local short range differences.[16] ^{13}C solid-state NMR spectra are presented in Figure 6. The chemical shift values of the alkyl chain of CGA did not exhibit significant differences for C2, C3, C4 and also for amide C6 atoms (Figure 6, Table S3, ESI†). The carboxylic acid C1 and C5 atoms showed peak values at 175.4, 179.4 ppm in Form-I whereas in Form-II in addition to the C1 and C5 (175.3, 179.4 ppm) peak positions two extra peaks were observed at 177.33 and 181.7 ppm, which is due to the two molecules in the asymmetric unit of Form-II (from X-ray analysis).

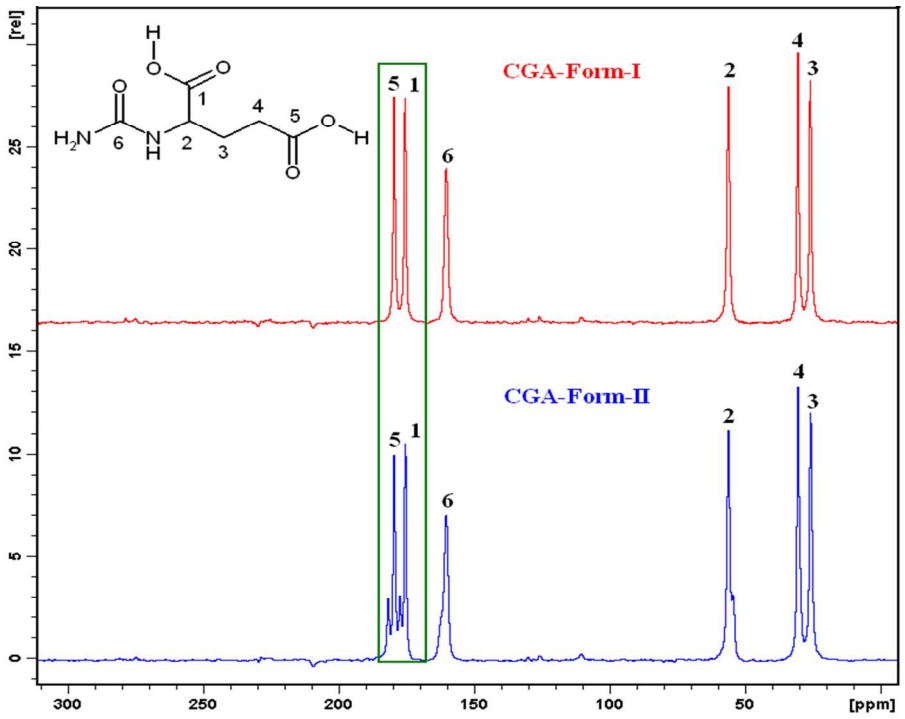

Figure 6 ^{13}C ss-NMR spectrum of CGA polymorphs shows that there is significant difference in chemical shifts. Multiple peaks for carboxylic C atoms in the Form-II are for the two molecules in the asymmetric unit (of the crystal structure).

Powder X-ray diffraction

CGA Forms-I and II are readily distinguishable by their unique powder XRD line patterns[17] (blue lines in Figure 7). The experimental PXRD pattern of commercial CGA matches with the calculated pattern of CGA Form-I (Figure S1, ESI†). Bulk material of novel Form-II prepared by rotovaporization exhibited unique powder diffraction line pattern that matches with the calculated pattern single crystal X-ray crystal structure for Form-II (Figure 7). The slight variations in the overlay of peaks of the experimental PXRD and the calculated lines of CGA-Form-II crystal structure is due to temperature effects; the experimental PXRD was recorded at room temperature and X-ray crystal structure reflections were collected at 100 K (Figure 7). The two polymorphs did not show any phase transformation up to heating at 160 °C in independent experiments as monitored by PXRD.

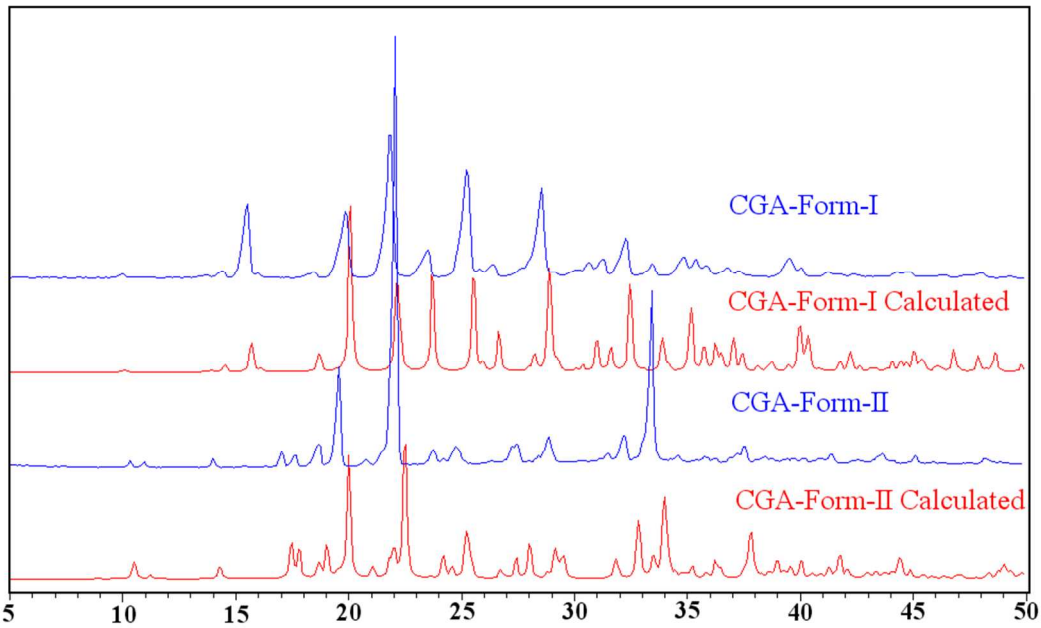

Figure 7 PXRD overlay of experimental patterns of the CGA forms exhibit unique powder lines and match to the calculated lines from the respective crystal structures.

Thermal and FESEM analysis

After confirming the bulk purity of the polymorphic materials, DSC analysis[18] was carried out to understand their thermodynamic relationship. No phase transformation was observed prior to melting at 167.9 °C for Form-I and 160.6 °C for Form-II (Figure 8, Table 3). The high melting polymorph Form-I has a higher heat of fusion (48.4 kJ/mol) while the lower melting polymorph Form-II has lower heat of fusion (36.5 kJ/mol), and hence both the polymorphs are monotropically related.[19] Both the forms were kept at 160 °C for 40 min in programmable oven to see the thermal effect; they were stable and no phase transformations were observed confirming the DSC measurements. Thus Form-I is the stable polymorph with higher enthalpy of fusion and higher melting point. The broad endotherm for Form-II was observed in multiple batches. Normally a broad endotherm in DSC implies that there is some other event such as, phase transformation, water evolution, occurring along with the melting process or due to low thermal conductivity of sample, kinetic effects, etc. The exact reason for a broad endotherm for Form-II but a sharp peak for Form-I is is not clear at the moment. What we did observe for both From-I and II is that heating the sample just beyond the melting point, cooling to room temperature and then re-heating did not show any DSC peak at the same temperature (Figure S2). This implies some kind of chemical transformation of the sample on heating.

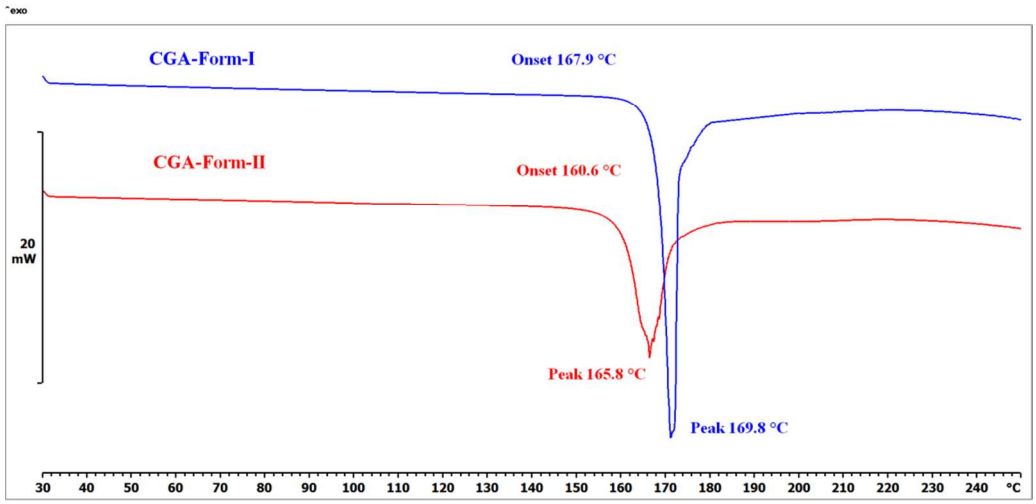

Figure 8 DSC thermograms of CGA Forms-I and II to show direct melting without any phase transition.

Table 3 Melting point and enthalpy values of CGA Forms.

CGA Forms	M.p. (°C) T_{onset}/ T_{peak}	ΔH_{fus} kJ/mol	Packing fraction (%)	Stability relation
CGA–Form-I	167.98/169.82	48.4	73.8	Monotropic, Form-I is thermodynamic
CGA–Form-II	160.61/165.79	36.5	69.4	

Field emission scanning electron microscopy is extremely informative for pharmaceutical solids to understand their morphology at the nm scale.[20] The individual polymorphs were spread uniformly on a carbon coated copper grid and then FESEM was recorded (Figure 9). Form-I appeared as needle and Form-II was found to be block morphology at 20 µm magnification scale, and these observed morphologies were in excellent match with those of the single crystals mounted for X-ray diffraction.

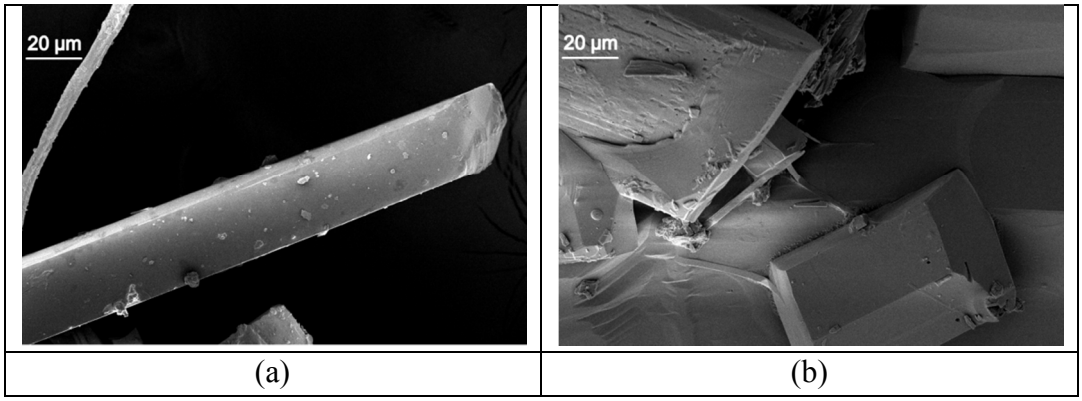

Figure 9 SEM images of CGA polymorphs (a) Form-I (b) Form-II to show the differences in morphology and bulk particles.

Hirshfeld surface and 2D fingerprint plots

Hirshfeld molecular surfaces[21] and the associated fingerprint plots generated using CrystalExplorer 3.0 on the basis of X-ray diffraction provides quantitative differences between polymorphs. The d_{norm} Hirshfeld surfaces are displayed using a red–white–blue color scheme, where red highlights shorter contacts, white is used for contacts around the van der Waals separation and blue is for longer contacts. The surfaces are shown as transparent to allow visualization of the orientation of the molecule and to show the conformational differences of the CGA molecules in both the Forms-I and II. Figure 10 presents Hirshfeld surfaces of the molecules in both the polymorphs. In Form-I, three large circular depressions (deep red) visible on the top left of the surface are indicative of hydrogen-bonding (O–H···O) contacts, and additional faint red circles one on top left and other is on right are from the N–H···O hydrogen bonds (Figure 10a). In general, the color intensity is high for stronger interactions, and this was observed for Form-I with shorter H-bonds (O–H···O: 1.63 Å, 167º, 1.72 Å, 176º; N–H···O: 1.90 Å, 167º, 2.09 Å, 147º). For Form-II (Figure 10b) there are three red regions on the left of the surface, two intense large circles due to the strong O–H···O (1.73 Å, 171º, 1.63 Å, 172º) and also from N–H···O (1.94 Å, 160º) bonds. Additional red regions at the left and right of the surface arise from the N–H···O (1.86 Å, 156º) and O–H···O (1.73 Å, 166º) contacts.

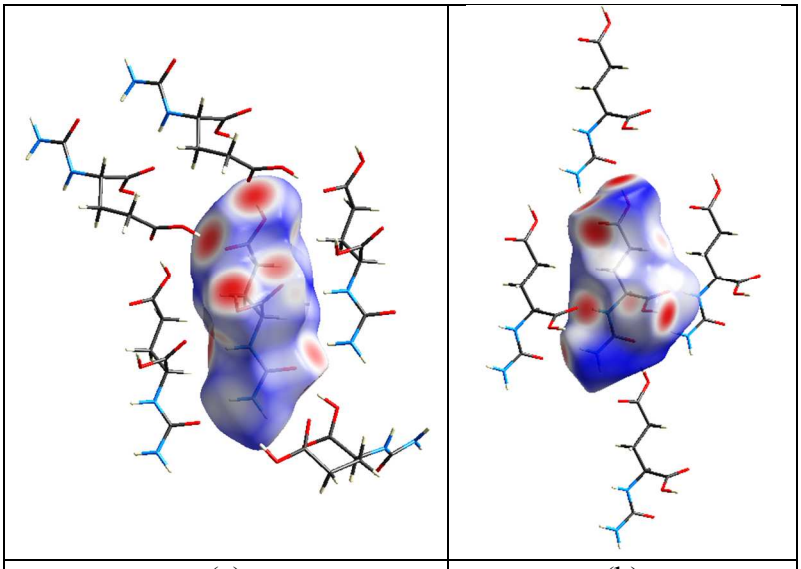

Figure 10 Hirshfeld surfaces with mapped d_{norm} property and neighboring molecules for (a) Form-I and (b) Form-II projected and transparency to show the conformation of the molecules in the forms.

Hirshfeld surfaces and fingerprint plots proved to be particularly suited for comparing environments of structures with $Z' > 1$ where the complex interplay between crystallographically

unique molecules could be rationalized in terms of the complementary surface regions. In Figure 11, d_i represents the distance from the surface to the nearest atom in the molecule itself, and d_e the distance to the nearest atom outside the molecule. In Form-I, presence of long sharp spikes towards the lower left corner near $d_e + d_i \approx 1.6$ Å of the plot indicates O···H interactions and it is a characteristics for strong hydrogen bonds resulting from for N−H···O and O−H···O and C−H···O hydrogen bonds (Figure 11). The contribution of these interactions to the Hirshfeld surfaces is 53.2% in Form-I (Figure 12). Two sharp spikes are present for Form-II as well, but because of two molecules in the asymmetric unit of Form-II structure, the contribution of O···H interactions increase (57.8% for molecule A and 56.6% for molecule B) (Figure 12). Overall there are more numerous short O···H interactions (from N−H···O, O−H···O, C−H···O) in Form-II. The wings for C−H···C interactions are slightly different for the two forms due to the different methylene CH atoms involved in C···H interactions, but their contribution is very low (2-3%) (Figure 12). The H··H interaction values are in a similar range (33% for Form-I and 31, 32% for Form-II). The calculated density and packing efficiency of the thermodynamic Form-I is higher (1.585 g cm^{-3}, 73.8%; vs. 1.496 g cm^{-3}, 69.4%).

	All interactions	O···H interactions	C···H interactions
Form-I	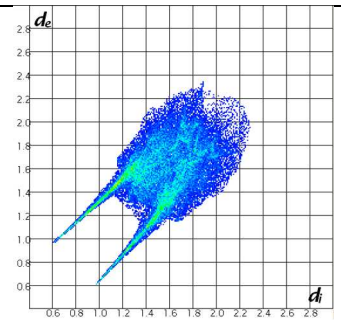	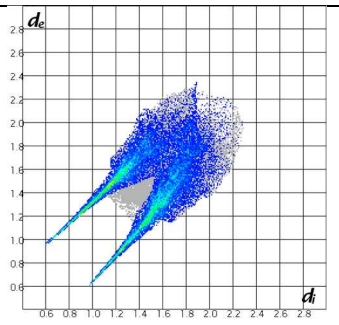	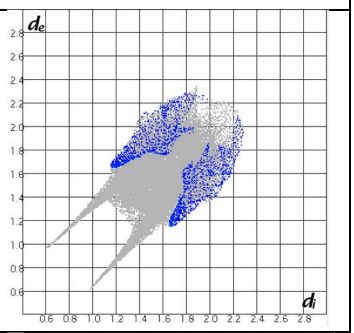
Form-IIA	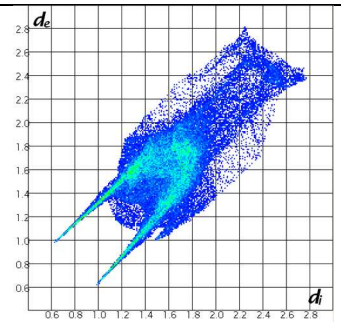	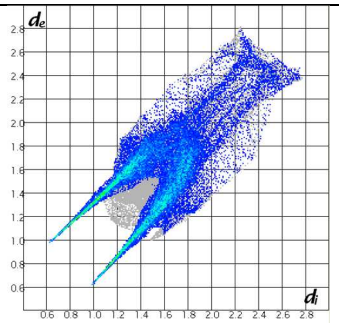	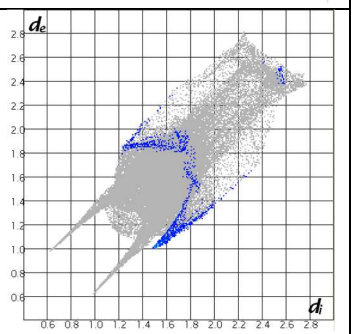
Form-IIB	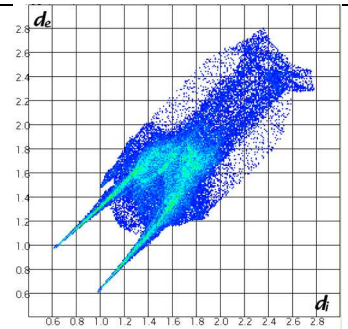	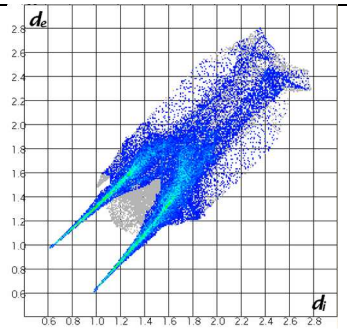	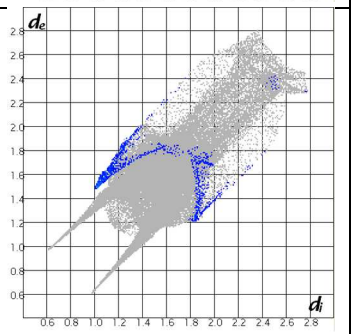

Figure 11 2D Hirshfeld fingerprint plots for Form-I and Form-II. Note that the A and B represent the two crystallographically independent molecules in Form-II.

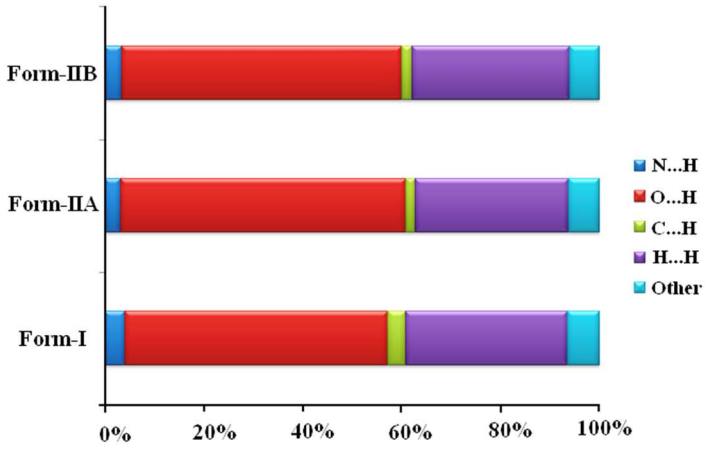

Figure 12 Contribution of major interactions to the Hirshfeld surface for Form-I and Form-II of CGA.

Grinding and solvent mediated transformations

The most suitable form for drug formulation is the one which exhibits an appropriate balance between solubility and stability. Therefore, it is important to establish the stability of polymorphic systems. Solution mediated polymorphic transformation is a fast, easy, and reliable method to determine the stable polymorph under conditions relevant to pharmaceutical tablets. Hence, slurry grinding experiments were performed on CGA polymorphs in a range of solvents, e.g. water, ethanol, pentane, alkaline pH 9.0 solution, and acetic acid pH 2.4 solution. Both the polymorphs were subjected to slurry grinding separately in these solvents to understand the effect of solvent on the stability outcome of solvent-mediated processes. Upon slurry grinding in water, ethanol, and pentane pure Form-I was stable for 48 h. Pure Form-II converted into Form-I in 10-12 h in water and ethanol but in pentane it took 24 h for conversion to Form-I (Figure S3, ESI†). Interestingly, slurry experiments on Form-I at alkaline pH 9.0 and acetic acid pH 2.4 solutions was found to convert to Form-II after 24 h, whereas Form-II under similar experimental conditions was found to be stable for 24 h. We did not observe trends such as non polar solvents preferentially give metastable form whereas polar solvents give stable forms,[22] however in our study alkaline pH 9.0 and acetic acid pH 2.4 solutions resulted in metastable Form-II. In competitive slurry experiments, wherein a mixture of the two forms was taken in 1:1 ratio, the product was pure Form-I (in water, ethanol, and pentane) after 8-10 h of slurry (Figure 13 and Figure S4, ESI†).

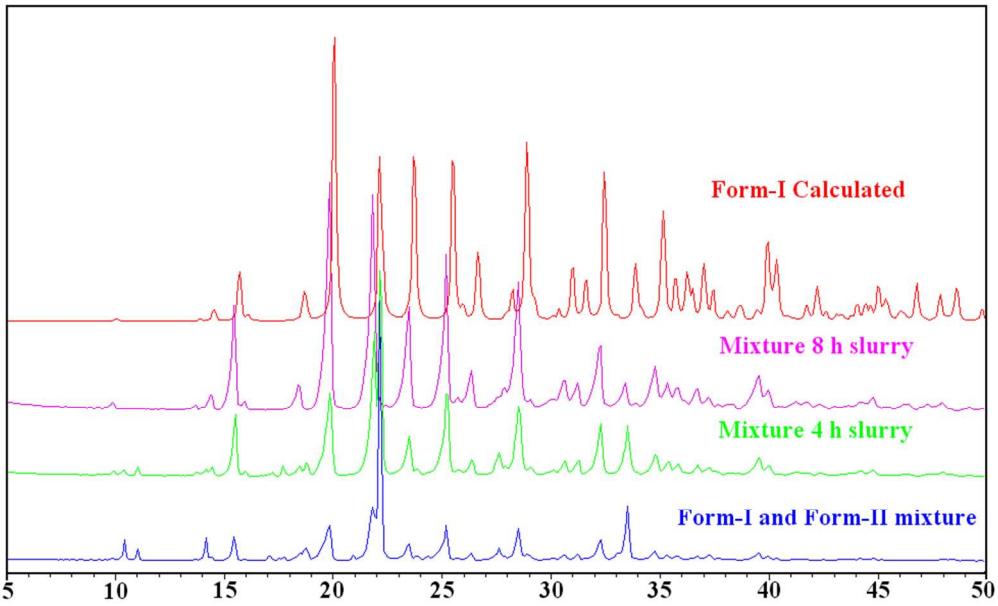

Figure 13 The mixture of Form-I and II (blue) was found to convert into Form-I (magenta) after slurry in EtOH solvent. The calculated PXRD pattern of Form-I (red) is shown for comparison.

Processing of solids can have a major impact on solid-solid phase transformations which consequently affects the dissolution of the crystal forms. Neat grinding/liquid assisted grinding (NG/LAG) at room temperature was carried out on CGA forms up to 1 h to gain an insight into mechanically activated polymorph conversion. Grinding is one process that has been shown to cause changes in polymorphs, and such a polymorphic transformation is often detrimental to the efficacy of the formulation for example, chloramphenicol palmitate[23] and ritonavir[24] cases. NG/LAG of pure Form-II was converted into Form-I upon grinding for 60 min (Figure 14). However, extended NG/LAG on Form-I for 2 h did not show any effect. In addition, competitive NG/LAG experiments on a mixture of forms gave the stable Form-I after 20 min (Figure 15).

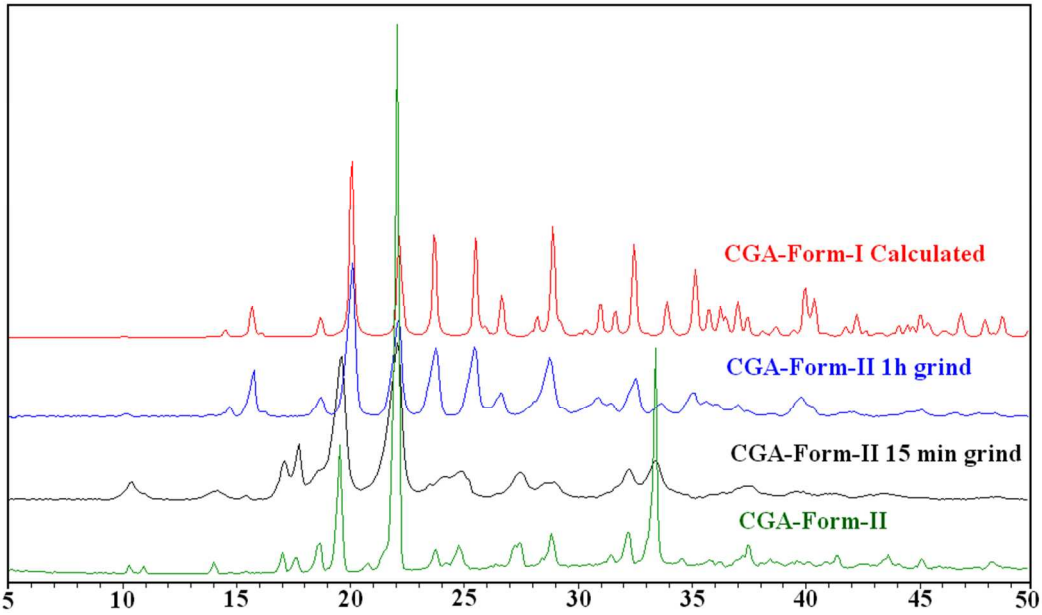

Figure 14 Overlay of experimental PXRD pattern of CGA-Form-II (green) with the ground material PXRD pattern of the same form, and Form-II was found to convert into Form-I after 1 h grinding. The calculated pattern of Form-I is shown for comparison (red).

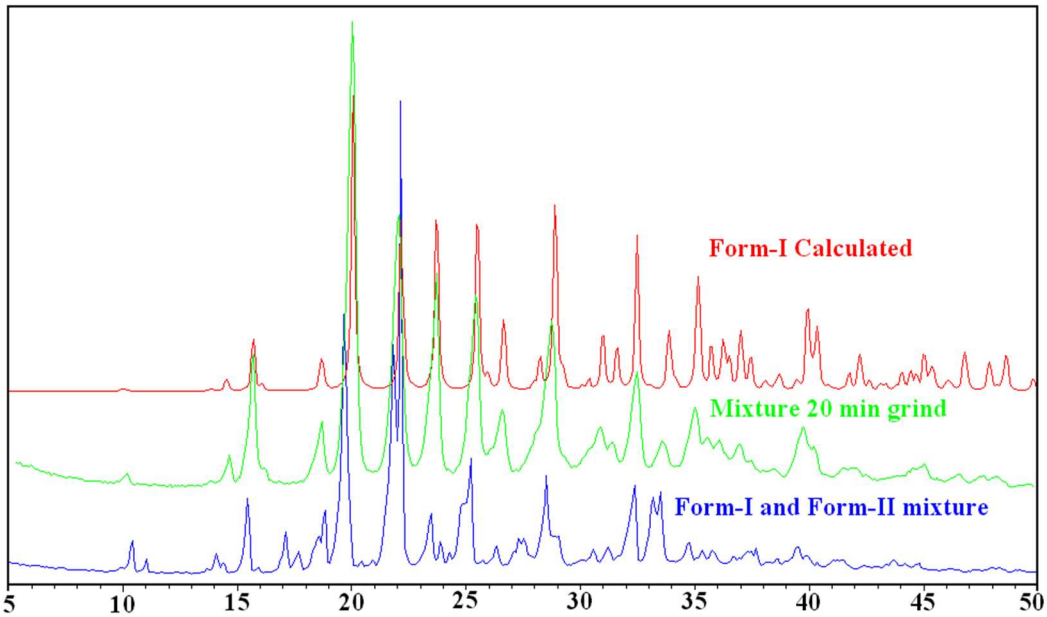

Figure 15 Overlay of experimental PXRD patterns of the mixture of Form-I and Form-II (blue), and the mixture was found to convert into Form-I after 20 min grinding (green). The calculated pattern of Form-I is shown for comparison (red).

Effect of humidity on CGA forms

Storage conditions of temperature and humidity affect the stability of pharmaceuticals.[25] In particular, hygroscopicity can have a significant impact on the physical and chemical stability of

active pharmaceutical ingredients (APIs). Therefore, it is important to know the physicochemical stabilities of different forms and the kinetics of their transformation at different humidity levels. Stability study for CGA polymorphs was carried out in accelerated ICH conditions of 40 °C and 75% RH. Both forms were found to be stable (no phase transformation or hydrate formation) for the test period of 2 months based on PXRD analysis (Figure 16). Whereas Form-I is thermodynamically stable, the fact that there was no change in Form-II also came as a surprise. At ambient conditions of Hyderabad (35 °C and 40% RH) the polymorphs are stable for more than six months.

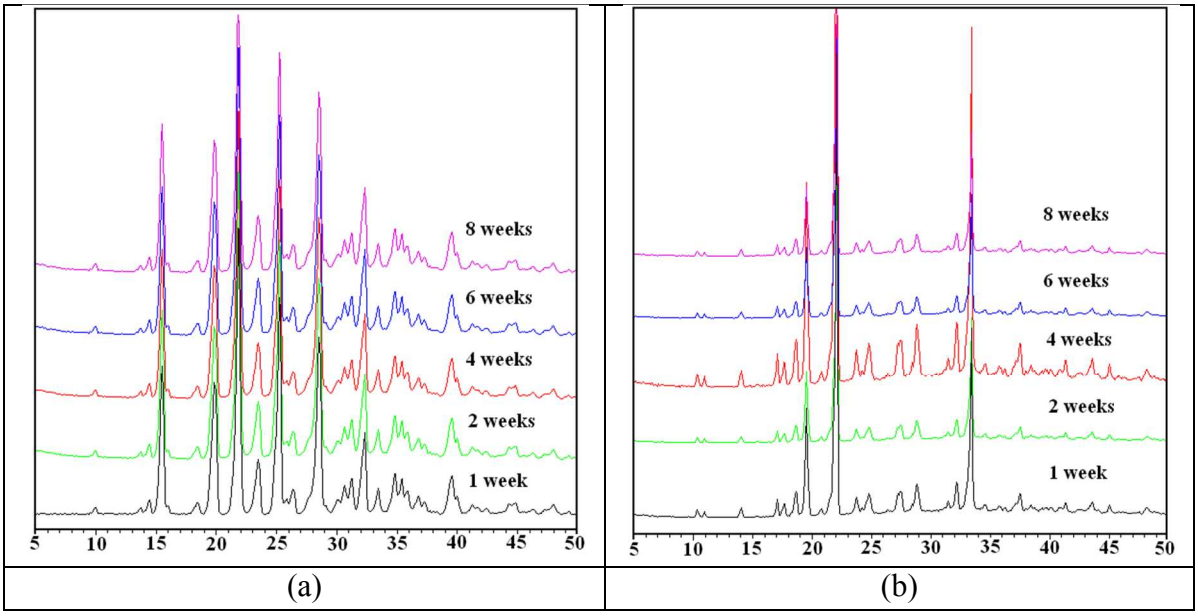

Figure 16 Overlay of PXRD patterns of (a) Form-I (b) Form-II after the **s**tability study at 40 °C and 75% RH shows that no form change/hydrate formation up to 2 months.

The study of hydration and dehydration of drug substances quantitatively is an important part of the investigations on polymorphs. This is achieved by measuring the water sorption-desorption isotherms on CGA polymorphs by Dynamic Vapor Sorption (DVS). Samples were subjected to a RH cycle of 10-90-10% at 40 °C (detailed in Experimental Section) and their water adsorption/ desorption behavior was analyzed. CGA-Form-II was found to adsorb 100.5% water at 90% RH and there was no significant percentage of water retention upon bringing down to 10% RH (Figure 17b). CGA-Form-I was found to be the least hygroscopic compared to Form-II (Figure 17a). Interestingly, moisture sorption profiles of both the forms showed somewhat different trends may be due to differences of the structure in the solid state. Water adsorption and desorption character of the solid materials depends on physical characteristics of the material, such as particle size, surface area, and pore size. From crystal structure analysis, both polymorphs have strong O–H···O and N–H···O hydrogen bonds, but the packing density of Form-II is lower, thereby leaving pores for water to enter uniformly during the sorption cycle (and leave during desorption), whereas the tighter packing of Form-I means that the behavior of

water sorption/desorption is erratic due to lattice reorganizations as water molecules interact with the crystal surface. Hence the DVS plots of polymorphs are different (Figure 17) but there is very small net gain/loss (<0.5%) of moisture by the sample.

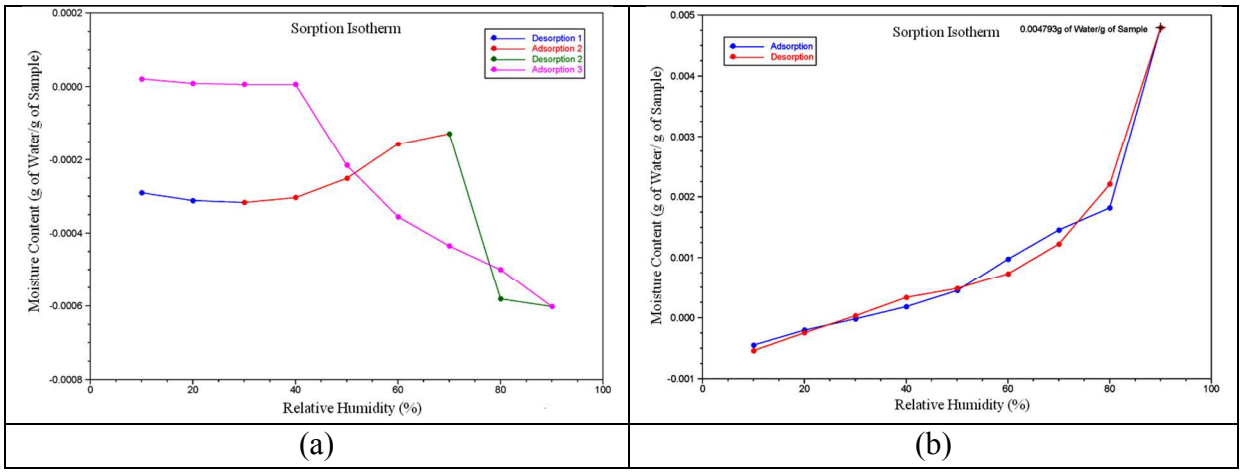

Figure 17 DVS isotherms of the CGA polymorphs show the stability towards moisture uptake for (a) Form-I, whereas (b) Form-II shows negligible (0.5%) water uptake at 90% RH but there is no retention of water after desorption.

Conclusions

Polymorph screening was carried out on the anti-hyperammonemic drug carglumic acid (CGA). In our search we found that two polymorphs Form-I and Form-II, and a degraded form hydantoin-5-propionic acid (5-HPA). We were successful in getting diffraction quality single crystals for all the forms and determined their X-ray crystal structures. The procedures were optimized to obtain each polymorph in bulk quantity for PXRD and DSC/DVS analysis. The main difference in synthons of these polymorphs is acid-acid catemer synthon in Form-I and acid-amide heterosynthon in Form-II. There are significant conformational differences between these synthon polymorphs. The higher density Form-I is thermodynamically stable and the dimorphs are monotropically related. The polymorphs were fully characterized by FT-IR, ^{13}C ss-NMR, DSC, FESEM, PXRD, and DVS techniques. Thermodynamic stability and phase transformations were established and furthermore the major intermolecular interactions in the two crystal structures were quantified through Hirshfeld surface analysis. Both polymorphs were stable for 2 months at ICH conditions of 40 ºC, 75% RH, and DVS analysis showed that Form-I is more stable to moisture than Form-II.

Experimental Section

Materials and Methods

Carglumic acid was purchased from Sigma-Aldrich (Hyderabad, India) and used without further purification. All other chemicals were of analytical or chromatographic grade. Water purified from a deionizer-cum-mixed-bed purification system (AquaDM, Bhanu, Hyderabad, India) was used in the experiments.

Preparation of CGA forms

CGA-Form-I

The commercial material obtained from Sigma-Aldrich matches to Form-I in our study which was confirmed by PXRD overlay. The bulk material in pure Form-I can also be obtained by slurry in EtOH, freeze drying in water. The bulk material was characterized by FT-IR, ^{13}C ss-NMR, PXRD and DSC. Single crystals suitable for X-ray diffraction were obtained upon dissolving 30 mg of CGA in 10 mL hot MeOH : 2-butanone (1:1 v/v) solvent mixture and left for slow evaporation at ambient conditions. Colorless needle crystals suitable for X-ray diffraction were obtained after 3-4 d upon solvent evaporation. M.p. 170-172 ºC.

CGA-Form-II

Form-II was obtained in bulk upon dissolving 100 mg of CGA commercial material in 20 ml of water: acetone (1:5 v/v) solvent mixture and heated until to obtain clear saturated solution. This solution was subjected to the rotoevaporation until the complete removal of solvent and the resultant material was kept at high vacuum of 30 min to result in dry powder material. This powder material was confirmed as Form-II by FT-IR, ^{13}C ss-NMR, PXRD and DSC. Colorless single crystals were obtained upon dissolving 30 mg of CGA in 12 mL hot CH_3CN: m-cresol (1:1 v/v) solvent mixture and left for slow evaporation at ambient conditions. Colorless block crystals suitable for X-ray diffraction were obtained after 3-4 d upon solvent evaporation. M.p. 166-168 ºC.

Hydantoin-5-propionic acid (5-HPA)

The degraded form (5-HPA) of CGA was obtained upon dissolving 30 mg of CGA commercial material in 10 ml of 2-butanone: propionic acid (1:1 v/v) solvent mixture and heated until to obtain clear solution. The solution filtered and left for slow evaporation at ambient conditions. Colorless needle crystals suitable for X-ray diffraction were obtained after 4-5 d upon solvent evaporation. M.p. 170-152 ºC.

Vibrational spectroscopy

Thermo-Nicolet 6700 Fourier transform infrared spectrophotometer with NXR-Fourier transform Raman module (Thermo Fisher Scientific, Waltham, Massachusetts) was used to record IR spectra. IR spectra were recorded on samples dispersed in KBr pellets. Data was analyzed using the Omnic software (Thermo Fisher Scientific, Waltham, Massachusetts).

Solid-state NMR spectroscopy

Solid-state ^{13}C NMR (ss-NMR) spectroscopy provides structural information about differences in hydrogen bonding, molecular conformations, and molecular mobility in the solid state.[16] The solid-state ^{13}C NMR spectra were obtained on a Bruker Ultrashield 400 spectrometer (Bruker BioSpin, Karlsruhe, Germany) utilizing a ^{13}C resonant frequency of 100 MHz (magnetic field strength of 9.39 T). Approximately 100 mg of crystalline sample was packed into a zirconium rotor with a Kel-F cap. The cross polarization, magic angle spinning (CP-MAS) pulse sequence was used for spectral acquisition. Each sample was spun at a frequency of 5.0 ± 0.01 kHz and the magic angle setting was calibrated by the KBr method. Each data set was subjected to a 5.0 Hz line broadening factor and subsequently Fourier transformed and phase corrected to produce a

frequency domain spectrum. The chemical shifts were referenced to TMS using glycine ($\delta_{glycine}$ = 43.3 ppm) as an external secondary standard.

Differential Scanning Calorimetry (DSC)

DSC was performed on a Mettler Toledo DSC 822e module. Samples were placed in crimped but vented aluminium sample pans. The typical sample size is 3-5 mg, and the temperature range is 30-250 °C @ 5 °C min^{-1}. Samples were purged by a stream of dry nitrogen flowing at 80 mL min^{-1}.

Field Emission Scanning Electron Microscope (FESEM)

The shape and morphology of the CGA forms were examined on a Carl Zeiss model Merlin Compact 6027 FESEM with a beam voltage of 3.0 kV. The sample was spread on a carbon-coated copper grid. Prior to FESEM imaging, an ultrathin layer of gold was coated in order to enhance the conductivity of the sample.

Dynamic Vapor Sorption (DVS)

Dynamic vapor sorption (DVS) was used to obtain sorption–desorption kinetic data of CGA polymorphs. DVS measurements were performed using a Q5000SA vapor sorption analyzer (TA Instruments, Delaware, USA) at 40°C. About 4-10 mg of the sample was placed in a metalized quartz sample pan and subjected to relative humidity flux from 10% RH to 90% RH and back to 10% RH with a step size of 10% change in humidity. A dwell time of 60 min was set for a weight change of >0.1% in the adsorption/desorption phase at a particular RH (5 min dwell time for a weight change of <0.1%). Thus, if the weight loss/gain is >0.1% at a particular RH, the instrument maintains the same RH for 60 min and then automatically sets at the next higher/lower value. If the weight gain/loss is <0.1%, the DVS cycle (10%–90%–10%) will be completed within 2 hours, otherwise it will take a longer duration.

X-ray crystallography

X-ray reflections for Form-I and Form-II were collected at 100 K on Bruker SMART-APEX CCD diffractometer equipped with a graphite monochromator and Mo-Kα fine-focus sealed tube (λ = 0.71073 Å). Data reduction was performed using Bruker SAINT Software.[26] Intensities were corrected for absorption using SADABS,[27] and the structure was solved and refined using SHELX-97.[28] X-ray reflections for hydantoin-5-propionic acid (5-HPA) was collected at 298 K on Oxford Xcalibur Gemini Eos CCD diffractometer using Mo−Kα radiation (λ = 0.7107 Å). Data reduction was performed using CrysAlisPro (version 1.171.33.55)[29] and OLEX2-1.0[30] was used to solve and refine the structures. All non-hydrogen atoms were refined anisotropically. Hydrogen atoms on heteroatoms were located from difference electron density maps and all C−H hydrogens were fixed geometrically. Hydrogen bond geometries were determined in Platon.[31] X-Seed[32] was used to prepare packing diagrams. Crystal structures are deposited as part of the Supporting Information and may be accessed at www.ccdc.cam.ac.uk/data_request/cif (CCDC Nos. 1043890-1043892).

Powder X-ray diffraction

Powder X-ray diffraction of all the samples were recorded on Bruker D8 Advance diffractometer (Bruker-AXS, Karlsruhe, Germany) using Cu-Kα X-radiation (λ= 1.5406 Å) at 40 kV and 30

mA power. X-ray diffraction patterns were collected over the 2θ range 5-50° at a scan rate of 1º min^{-1}. Powder Cell 2.4[33] (Federal Institute of Materials Research and Testing, Berlin, Germany) was used for Rietveld refinement of experimental PXRD and calculated lines from the X-ray crystal structure.

Acknowledgements

D. M. thanks CSIR for fellowship. We thank the Department of Science and Technology for J. C. Bose fellowship SR/S2/JCB-06/2009, DST-SERB Scheme Novel solid-state forms of API's SR/S1/OC-37/2011 for funding. DST (IRPHA, PURSE) and University Grants Commission (UPE) are thanked for providing the instrumentation and infrastructure facilities at UOH.

References

1. (a) L. Caldovic, H. Morizono, Y. Daikhin, I. Nissim, R. J. McCarter, M. Yudkoff, M. Tuchman, *J. Pediatr*., 2004, **145**, 552–554; (b) O. Elpeleg, A. Shaag, E. Ben-Shalom, T. Schmid, C. Bachmann, *Ann. Neurol.*, 2002, **52**, 845–849; (c) J. V. Leonard, M. P. W. Platt, A. A. Morris, *Eur. J. Pediatr*. 2008, **167**, 305–309.
2. (a) J. Häberle, *Ther. Clin. Risk Manag.*, 2011, **7**, 327–332; (b) J. E. O'Connor, A. Jordá, S. Grisolia, *Eur. J. Pediatr.*, 1985, **143**, 196–197.
3. M. Daniotti, G. la Marca, P. Fiorini, L. Filippi, *Int. J. Gen. Med.*, 2011, **4,** 21–28.
4. ChemSpider: Chemical structure database freely distributed by the RSC, www.chemspider.com.
5. (a) M. Abacan, A. Boneh, *Mol. Genet. Metab.*, 2013, **109**, 397–401; (b) C. Bachmann, S. Krähenbühl, J. P. Colombo, G. Schubiger, K. H. Jaggi, O. Tönz, *N. Engl. J. Med.*, 1981, **304**, 543–543; (c) J. P. Colombo JP, *Adv. Exp. Med. Biol.*, 1994, **368**, 135–143.
6. (a) A. J. Dobson, R. E. Gerkin, *Acta Crystallogr.*, 1997, C53, 73–76; (b) N. Kausar, B. D. Alexander, R. A. Palmer, B. S. Potter, T. J. Dines, M. Helliwell, B. Z. Chowdhry, *J. Chem. Crystallogr.*, 2010, **40**, 602–607.
7. Cambridge Structural Database, ver. 5.36. ConQuest 1.17, November 2014 release, November 2014 update, CCDC, www.ccdc.cam.ac.uk.
8. (a) G. R. Desiraju, *Crystal Engineering: The Design of Organic Solids*, Elsevier, Amsterdam, 1989; (b) G. R. Desiraju, *J. Chem. Sci.*, 2010, **122**, 667–675; (c) G. R. Desiraju, J. J. Vittal and A. Ramanan, *Crystal Engineering. A Textbook*, World Scientific, Singapore, 2011.
9. (a) L. F. Huang and W. Q. T. Tong, *Adv. Drug Del. Rev.*, 2004, **56**, 321–334; (b) T. L. Threlfall, *Analyst*, 1995, **120**, 2435–2460; (c) J. Bernstein, *Polymorphism in Molecular Crystals*, Clarendon, Oxford, 2002; (d) F. Fabbiani, D. Allan, S. Parsons and C. Pulham, *CrystEngComm*, 2005, **7**, 179–186; (e) P. Sanphui, N. Goud, U. Khandavilli, S. Bhanoth and A. Nangia, *Chem. Commun.*, 2011, **47**, 5013–5015; (F) J. Haleblian and W. J. McCrone, *Pharm. Sci.*, 1969, **58**, 911–929.
10. (a) P. P. Bag, M. Patni and C. M. Reddy, *CrystEngComm*, 2011, **13**, 5650–5652; (b) N. Shan, F. Toda and W. Jones, *Chem. Commun.*, 2002, 2372–2373; (c) A. V. Trask and W.

Jones, *Top. Curr. Chem*., 2005, **254,** 41–70; (d) A. Delori, T. Friščić and W. Jones, *CrystEngComm*, 2012, **14**, 2350–2362.

11. K. R. Morris, U. J. Griesser, C. J. Eckhardt and J. G. Stowell, *Adv. Drug Del. Rev.*, 2001, **48**, 91–114.
12. (a) R. D. B. Walsh, M. W. Bradner, S. Fleischman, L. A. Morales, B. Moulton, N. Rodriguez-Hornedo and M. J. Zaworotko, *Chem. Commun.*, 2003, **2**, 186–187. (b) G. R. Desiraju, *Angew. Chem., Int. Ed. Engl*., 1995, **34**, 2311–2327; (c) F. H. Allen, W. D. S. Motherwell, P. R. Raithby, G. P. Shields and R. Taylor, *New J. Chem.*, 1999, **23**, 25–34.
13. A. J. Cruz-Cabeza and J. Bernstein, *Chem. Rev.*, 2014, **114**, 2170–2191.
14. (a) M. C. Etter, *Acc. Chem. Res*., 1990, **23**, 120–126; (b) J. Bernstein, R. E. Davis, L. Shimoni and N. L. Chang, *Angew. Chem., Int. Ed. Engl.*, 1995, **34**, 1555–1573.
15. (a) R. M. Silverstein, *Spectrometric Identification of Organic Compounds*, 6th Ed., John Wiley, New York, 2002; (b) E. Smith and G. Dent, *Modern Raman Spectroscopy, A Practical Approach*, John Wiley, New York, 2005.
16. (a) F. G. Vogt, J. S. Clawson, M. Strohmeier, A. J. Edwards, T. N. Pham and S. A. Watson, *Cryst. Growth Des.*, 2008, **9**, 921–937; (b) A. E. Aliev and K. D. M. Harris, *Supramolecular Assembly via Hydrogen Bonds I*, 2004, 1–53; (c) A. W. Newman, S. L. Childs and B. A Cowans, Salt Cocrystal Form Selection, In *Preclinical Development Handbook*, John-Wiley, Hoboken, 2008, 455–481.
17. (a) H. B. Brittain, *Am. Pharm. Rev.*, 2002, **5**, 74–80; (b) G. P. Stahly, *Cryst. Growth Des.*, 2007, **7**, 1007–1026.
18. (a) J. L. Ford, P. Timmins, *Pharmaceutical Thermal Analysis: Techniques and Applications*, E. Horwood, Chichester, 1989; (b) H. G. Brittain, *Polymorphism in Pharmaceutical Solids*, Marcel Dekker, New York, 1999.
19. (a) A.Burger and R. Ramberger, *Mikrochim. Acta II*, 1979, 259–271.
20. (a) M. Veverka, P. Simon, J. Lokaj and E. Veverkova, *Monatsh. Chem.*, 2012, **143**, 65−71; (b) R. Barbas, R. Prohens and C. Puigjaner, *J. Therm. Anal. Calor.*, 2007, **89**, 687−692; (c) J. Mensah and K. Kim, *Chem. Eng. Trans.*, 2013, **32**, 2221−2226.
21. (a) M. A. Spackman and D. Jayatilaka, *CrystEngComm*, 2009, **11**, 19–32; (b) J. J. McKinnon, D. Jayatilaka and M. A. Spackman, *Chem. Commun.*, 2007, 3814–3816; (c) J. Bernstein, *Cryst. Growth Des.*, 2011, **11**, 632–650; (d) F. P. A. Fabbiani, L. T. Byrne, J. J. McKinnon and M. A. Spackman, *CrystEngComm*, 2007, **9**, 728–731.
22. (a) V. Trask, A. W. S. Motherwell and W. Jones, *Chem. Commun*., 2004, 890–891; (b) S. Aitipamula, P. S. Chow and R. Tan, *CrystEngComm*, 2010, **12**, 3691–3697; (c) M. D. Eddleston, S. Sivachelvam and W. Jones, *CrystEngComm*, 2013, **15**, 175–181.
23. J. Bernstein, *NATO Sci. Ser., II Mathematics, Phys. Chem.*, 2002, **68**, 244–249.
24. C.-H. Gu, V. Young Jr. and D. J. W. Grant, *J. Pharm. Sci.*, 2001, **90**, 1878–1890.
25. (a) N. V. Phadnis and R. Suryanarayanan, *J. Pharm. Sci*., 1997, **86**, 1256–1263; (b) M. Otsuka, R. Teraoka and Y. Matsuda, *Pharm. Res.*, 1991, **8**, 1066–1068; (c) Y. Hu, A. Erxleben, B. K. Hodnett, B. Li, P. McArdle, Å. C. Rasmuson and A. G. Ryder, *Cryst.*

Growth Des., 2013, **13**, 3404–3413; (d) M. Otsuka, M. Onoe and Y. Matsuda, *Pharm. Res.* 1993, **10**, 577–582.

26. *SAINT-Plus*, version 6.45; Bruker AXS Inc., Madison, Wisconsin, U.S.A., **2003**.
27. SADABS, *Program for Empirical Absorption Correction of Area Detector Data*; G. M. Sheldrick, University of Göttingen: Göttingen, Germany, **1997**.
28. (a) *SMART*, version 5.625 and *SHELX-TL*, version 6.12, Bruker AXS Inc.: Madison, Wisconsin, USA, **2000**; (b) G. M. Sheldrick, *SHELXS-97* and *SHELXL-97*; University of Göttingen: Göttingen, Germany, **1997**.
29. *CrysAlis CCD and CrysAlis RED*, Ver. 1.171.33.55; Oxford Diffraction Ltd: Yarnton, Oxfordshire, U.K., **2008**.
30. O. V. Dolomanov, A. J. Blake, N. R. Champness and M. Schröder, *J. Appl. Crystallogr.*, 2003, **36**, 1283–1284.
31. A. L. Spek, *PLATON, A Multipurpose Crystallographic Tool*; Utrecht University: Utrecht, Netherlands, **2002**.
32. L. J. Barbour, *X-Seed*, *Graphical Interface to SHELX-97 and POV-Ray*, *Program for Better Quality of Crystallographic Figures*; University of Missouri-Columbia, Missouri, U.S.A., **1999**.
33. Powder Cell, A Program for Structure Visualization, Powder Pattern Calculation and Profile Fitting, http://www.ccp14.ac.uk/index.html, **2013**.

TOC

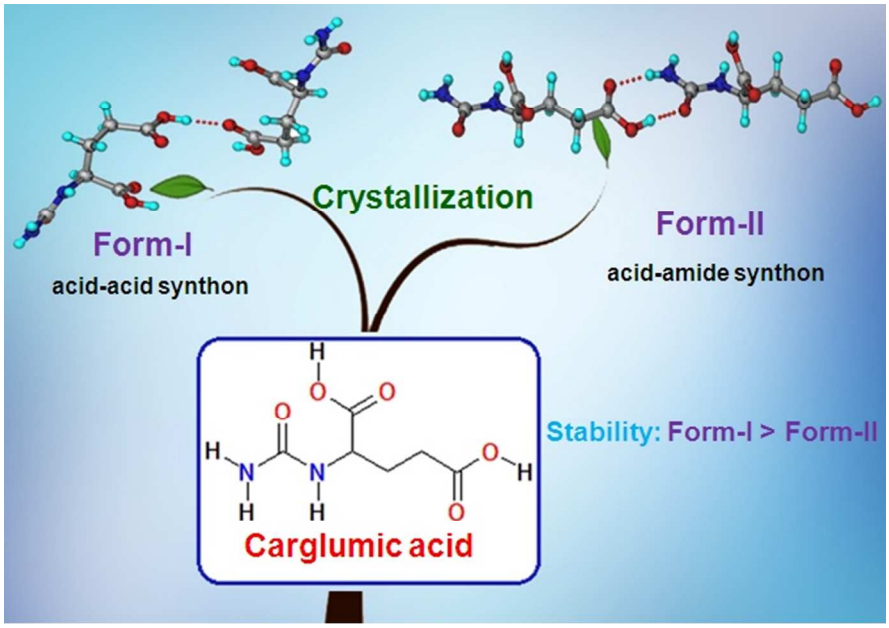

Solid form screen of anti-hyperammonemic drug carglumic acid (CGA) resulted in two polymorphs, Form-I and Form-II. The crystal structure of Form-I is sustained by acid catemer synthon whereas Form-II has acid-amide heterosynthon. Slurry grinding, thermal stress, stability measurements, and DVS analysis confirm the thermodynamic stability of Form-I.